EXPERIMENTAL DATA ON CHF FOR FORCED CONVECTION WATER BOILING IN LONG HORIZONTAL CAPILLARY TUBES

A.M. Lezzi[†], A. Niro[‡] and G.P. Beretta[†]

[†]Dipartimento di Ingegneria Meccanica, Università di Brescia
via Branze 38, 25123 Brescia, Italy

[‡]Dipartimento di Energetica, Politecnico di Milano
p.le L. da Vinci 32, 20133 Milano, Italy

Heat Transfer 1994

Proceedings of
The Tenth International
Heat Transfer Conference

Brighton, UK

Volume 7

Natural convection
Applied heat transfer
Flow boiling

Edited by
G.F. Hewitt

in cooperation with the members of the
International Scientific Committee:

M. Combarnous, M. Cumo, E. Hahne,
G. Hetsroni, C.J. Hoogendoorn,
J.R. Howell, A.I. Leontiev, J.S. Lee,
L.F. Milanez, P. Oosthuizen, V.M.K. Sastri,
K. Suzuki, B.X. Wang

EXPERIMENTAL DATA ON CHF FOR FORCED CONVECTION WATER BOILING IN LONG HORIZONTAL CAPILLARY TUBES

A.M. Lezzi†, A. Niro‡ and G.P. Beretta†

†Dipartimento di Ingegneria Meccanica, Università di Brescia
via Branze 38, 25123 Brescia, Italy

‡Dipartimento di Energetica, Politecnico di Milano
p.le L. da Vinci 32, 20133 Milano, Italy

ABSTRACT

We present experimental results on critical heat flux in forced convection boiling of water in a horizontal capillary tube with inner diameter $D = 1$ mm, for L/D ratio approximately equal to 250, 500, and 1000. Data are for: low mass fluxes, between 800 and 2700 kg/m^{2}s; pressures between 1.9 and 7.2 MPa; and inlet conditions between saturation and strong subcooling. In all cases fluid exit quality is high and critical heat flux is reached through dryout. Results are compared with extrapolations of the Katto correlation.

1. INTRODUCTION

Flow boiling in capillary tubes has been recognized lately (Hosaka *et al.* 1990) as a promising technique in heat transfer enhancement. For example, in compact heat exchangers, high power exchange per unit volume is usually achieved by means of extended surfaces with very large contact area. An alternative to finned tubes, however, as suggested by Echigo *et al.* (1992), is to use small diameter tubes to increase the contact area per unit volume. Flow boiling in capillary tubes may find applications also in cooling of electronic power components.

In the literature, data on critical heat flux for forced convection boiling in capillary tubes are scarce. Bergles (1963) investigated CHF in tubes with inner diameter as small as 0.6 mm and found that CHF is enhanced by decreasing the tube diameter. This behaviour has been confirmed by much recent work related to fusion reactor technology (see, e.g., Celata 1993, Mishima *et al.* 1993). These data are all obtained under conditions of subcooled or low quality flow boiling at CHF location, when the mechanism responsible for the critical condition is known as departure from nucleate boiling (DNB).

An entirely different mechanism is at work for high exit quality flows. The flow pattern is annular and CHF condition is caused by the drying out of the liquid film. Existing correlations for high quality CHF predict a slight increase of the critical heat flux with the decrease of the tube diameter for fixed length-to-diameter ratio. However, these correlations are valid for diameters greater than a few millimeters. Work is needed to clarify the role of capillarity effects on the CHF in the high quality region.

In this study, we present experimental results on CHF in flow boiling of water in long horizontal capillary tubes with inner diameter $D = 1$ mm and heated length ranging between 0.25 to 1 m, approximately. CHF data are for low mass fluxes (between 800 and 2700 kg/m^{2}s); intermediate outlet pressures (between 1.9 and 7.2 MPa); and subcooled inlet conditions varying from 0 up to 250 K. In all cases the fluid quality at the tube outlet is higher than 0.6 and critical heat flux is reached through dryout.

Results are compared with extrapolations of the Katto correlation (as proposed by Katto and Ohno 1984). Agreement of the data with the values predicted by the Katto correlation seems to suggest that, at least for low mass fluxes and tube diameters down to 1 mm, the effect of tube diameter on CHF for water does not differ from that characteristic of larger diameters.

2. EXPERIMENTAL APPARATUS

Figure 1 shows a schematic diagram of the experimental apparatus. Demineralized water is drawn from a tank by a volumetric pump with maximum volume flow rate of 11 dm^3/h. Pressurized water flows through a 5 dm^3, AISI 316 stainless steel damper (based on cold water compressibility only) which reduces pressure oscillations to less than 3%. This type of damper was replaced with 0.3 dm^3, bladder-type accumulator, pressurized with nitrogen (residual pulsation $< 1\%$). The latter damper was used only in the tests with heated length equal to 0.25 and 0.5 m.

The preheating section is a horizontal, 3.5 m long, 1 mm i.d., 0.5 mm wall thickness, AISI 304 stainless steel tube heated uniformly by Joule effect using a max 100 A, 2.5 kW, d.c., switch mode power supply. A 10 cm long, 0.5 mm i.d. tube at the section exit provides a further pressure drop by which saturation conditions can be reached at the test section entrance with no boiling in the preheating section. The test section is a horizontal, straight, 1 mm i.d., 0.25 mm wall thickness, AISI 304

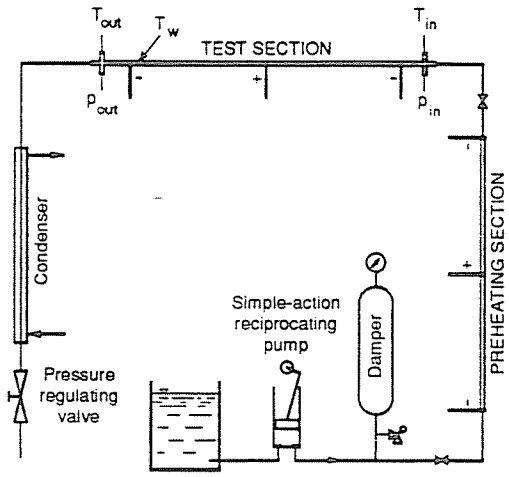

Figure 1. Schematics of the experimental apparatus.

stainless steel tube with smooth inner surface. It is heated uniformly by Joule effect using a max 200 A, 5 kW, d.c. power supply.

For both the preheating and the test section, three copper clamps brazed at the two extremes and at the center as shown in the figure provide the electric current to the tube and also its mechanical support. The electric power supplied to the test section is computed by multiplying the measured voltage drop across the heated tube length and the current flowing through the tube walls. The current is evaluated by measuring the voltage drop across a precision shunt resistor.

About 1 cm upstream of the downstream copper clamp of the test section, a K-type thermocouple is spot-brazed on the outside wall. This temperature reading (T_w) signals when critical heat flux is reached. The tube length L is defined as the heated length between the upstream copper clamp and the wall thermocouple. Four test sections are used in the present study with length L equal to 239, 241, 502, and 975 mm, respectively.

The test section is mounted between two 4-way 1/8" cross fittings. Each such fitting, on one side is connected via 1/8" piping to an absolute pressure transducer, and on the opposite side provides access for a 0.5 mm J-type thermocouple mounted with its junction at the centerline of the water flow across the fitting. These measurements (p_{in}, p_{out}, T_{in}, T_{out}) are important to evaluate inlet water pressure and subcooling, exit pressure at critical heat flux, and heat loss. The distance between the wall thermocouple where CHF condition is detected, and the location in the downstream fitting where p_{out} and T_{out} are measured is about 4 cm. Also the upstream copper clamp is brazed about 4 cm from the upstream 4-way cross fitting, so as to provide, before the heated length of the test section, about 40 diameters of unheated length to allow full development of the water velocity profile.

Downstream of the test section, the flow passes through the inner tube of a counterflow double-pipe condenser and is cooled down to ambient temperature. Based on previous experience (Bertoletti *et al.* 1965), in order to avoid possible oscillations at CHF, the condenser inner tube is designed with a limited cross section so as to leave for the vapor phase a volume comparable to that of the test section. Indeed, no oscillations affect the data presented in this study. Finally, the flow goes through a pressure regulating valve which is operated manually.

3. EXPERIMENTAL PROCEDURE

The voltages across the preheating and the test sections, and the shunt resistors, as well as the thermocouple voltages corresponding to T_{in}, T_{out}, T_w and the pressure transducer signals are read in a 5-second cycle by a data acquisition unit, and sent to an on-line PC for storage and visualization.

The experimental procedure consists of the following actions. First, the pump flow rate is preset by using the manual control and the exit valve is regulated to obtain the desired outlet pressure p_{out}. Then the preheating section power supply is turned on, and the power is gradually increased until the desired operating value of T_{in} is reached. A few minutes later, after thermal stabilization of the system, also the test section power supply is turned on and the power gradually increased to approach CHF conditions. Small adjustments of pressure and preheating power allow regulation of outlet pressure and inlet subcooling as desired. Again, after thermal stabilization, the test section power is increased at small increments and long time intervals. At any power step the reading of T_w varies very little below CHF, whereas above CHF it increases significantly with further power increase, clearly indicating that CHF has been exceeded.

The data collected during an experimental run are post-processed in order to determine the power supplied to the test section at CHF condition. The time history of test section and preheating section power is inspected to identify any change larger than a prescribed threshold (15 W). Then the average and the standard deviation of data recorded between two consecutive variations are computed.

As test section power is increased the following events are observed. At first, T_w remains practically constant with a standard deviation smaller than 1 K. As CHF condition is approached, T_w exhibits fluctuations characterized by a standard deviation between 1 and 10 K. A 1 or 2 K increment of the average value of T_w is common at this stage. Eventually T_w begins to increase substantially at any power increment.

An average value of T_w 5 K larger than the practically constant pre-crisis value is adopted as a criterion for detecting the onset of CHF condition. Since the test section is not thermally insulated, the power determined in this way is corrected by subtracting the heat loss due to radiation and natural convection around the test channel, and to conduction through the copper clamps and the unheated entrance and exit lengths. The error made in calculating the heat losses is estimated within 10 W, which is equivalent to a relative error smaller than 1% in

determining the actual power supplied to the fluid.

The mass flow rate G is calculated from the pump characteristic curves using the pressure read by a manometer placed between the pump and the damper. To assess the accuracy of this procedure, in a few test cases the mass flow rate was measured by direct weighing of the water outflow over a period of time. The differences found in this way were within 3%.

Temperatures are converted from thermocouple voltages with ASTM standard calibrations. The standard limits of error at typical operating temperatures are within ± 2.2 K. The errors in pressure measurements are estimated within ± 0.05 MPa.

4. EXPERIMENTAL RESULTS

In this study we present experimental data obtained for water mass fluxes G between 800 and 2700 kg/m^{2}s (i.e., liquid water inlet velocities between 1.0 and 3.2 m/s); outlet pressures p_{out} between 1.9 and 7.2 MPa, clustered around three reference values, i.e., 3, 5, and 7 MPa; and with inlet thermodynamic conditions ranging between near saturation to strong subcooling, corresponding to inlet qualities $0 \geq x_{in} > -0.7$. The inlet quality is defined as $x_{in} = (h_{in} - h_l)/h_{lg}$, where h_l and h_{lg} are evaluated at inlet pressure p_{in}.

Table 1 lists for all experimental tests the critical heat flux $\dot{q}_c$ and the values of some measured or estimated quantities. The total number of tests amounts to 87.

A comparison with the flow pattern map proposed by Weisman *et al.* (1979) indicates that the flow is annular for most of the test section. At CHF the outlet quality is high and the local heat transfer characteristics deteriorate significantly but not destructively. The test section can operate steadily with no structural damage even at heat fluxes exceeding critical conditions.

In Figs. 2-4 the experimental data are examined in terms of their dependence on x_{in}, G, and p_{out}. As is well known, CHF usually exhibits a linear dependence on inlet subcooling. In order to verify this behaviour, in Fig. 2 a representative sample of our CHF data is plotted versus x_{in} for a fixed outlet pressure (5 MPa) and for several values of G and L. As is seen from the figure, the data correlate very well. This fact justifies disregarding subcooling effects in the following analysis. In Table 2, CHF values extrapolated at zero inlet quality are listed together with the corresponding mean values of L, G, and p_{out}.

In Fig. 3, CHF data are plotted versus water mass flux for three fixed conditions of nominal outlet pressure (3, 5 and 7 MPa) and $L = 975$ mm, whereas in Fig. 4, data are plotted versus outlet pressure for $L = 975$ mm. The effect of water mass flux is outlined grouping data within five narrow bands of G. All values of $\dot{q}_c$ plotted in Figs. 3 and 4 refer to inlet thermodynamic conditions of near saturation, x_{in} being always greater than -0.05 (subcoolings between 0 and 16 K). As is seen from Figs. 2-4, the data presented in this study show the same qualitative features of CHF

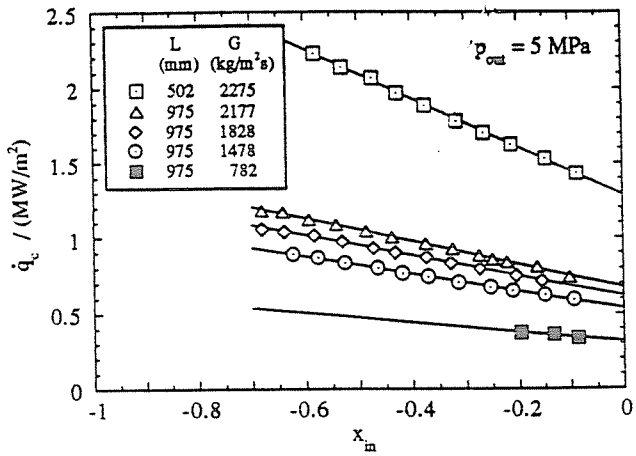

Figure 2. CHF data versus x_{in} for different G and L.

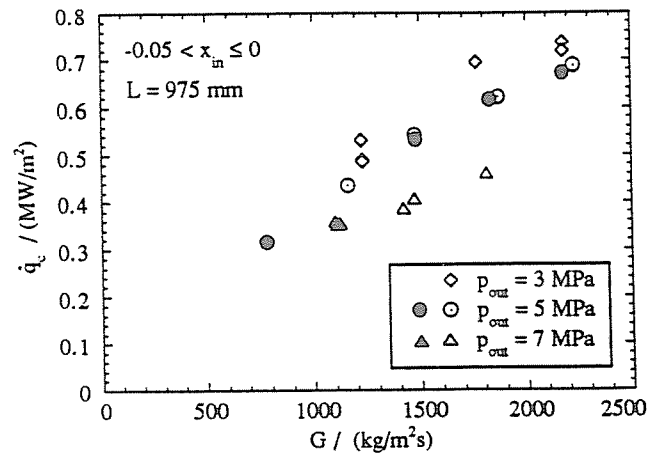

Figure 3. CHF data versus G for different p_{out} at inlet conditions of near saturation. Solid marks denote extrapolated points from Table 2.

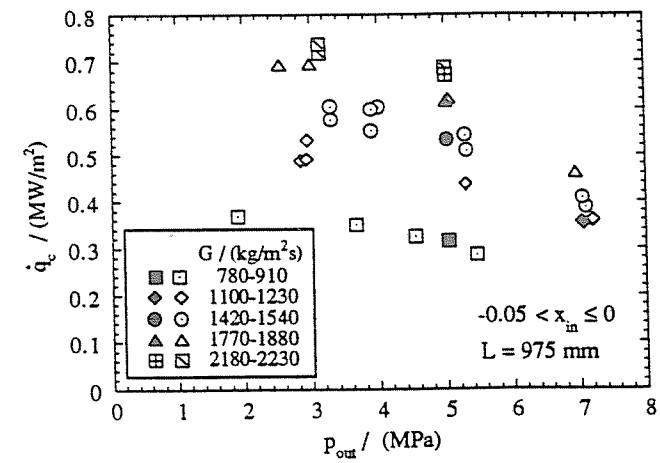

Figure 4. CHF data versus p_{out} for different G. Solid marks denote extrapolated points from Table 2.

Table 1. Summary of measured and estimated quantities at CHF

G kg/m^{2}s	p_{in} MPa	T_{in} °C	x_{in}	p_{out} MPa	x_{out}	$\dot{q}_c$ MW/m^2
	$D = 1$ mm		$L = 0.239$ m			
1480	7.18	258.6	-0.10	7.01	0.82	2.052
1480	7.15	230.4	-0.19	6.97	0.82	2.257
1475	7.20	213.2	-0.24	7.03	0.82	2.363
	$D = 1$ mm		$L = 0.241$ m			
1491	7.13	249.0	-0.13	6.96	0.81	2.079
1496	7.13	230.1	-0.19	6.96	0.80	2.206
	$D = 1$ mm		$L = 0.502$ m			
1485	7.29	266.8	-0.08	7.05	0.72	0.869
1475	7.29	248.1	-0.14	7.05	0.71	0.914
1475	7.24	230.1	-0.19	7.03	0.71	0.976
1464	7.26	213.2	-0.25	7.03	0.71	1.021
1464	7.21	190.1	-0.31	7.00	0.71	1.098
2270	5.65	244.0	-0.09	4.98	0.72	1.431
2270	5.65	223.1	-0.15	4.97	0.72	1.534
2270	5.66	200.5	-0.21	5.03	0.71	1.628
2270	5.64	181.5	-0.26	5.02	0.70	1.704
2270	5.58	161.4	-0.32	4.98	0.69	1.783
2270	5.59	140.0	-0.37	4.98	0.69	1.886
2270	5.59	120.6	-0.43	5.00	0.68	1.968
2303	5.57	102.5	-0.47	5.00	0.67	2.067
2281	5.58	81.2	-0.53	5.03	0.67	2.138
2281	5.56	60.8	-0.58	5.03	0.66	2.227
2738	5.87	198.6	-0.23	5.03	0.66	1.873
	$D = 1$ mm		$L = 0.975$ m			
776	5.65	268.6	-0.01	5.45	0.90	0.285
782	5.29	238.8	-0.09	5.08	0.97	0.338
782	5.04	219.0	-0.13	4.96	0.99	0.364
782	5.25	199.2	-0.20	5.04	0.97	0.374
816	4.75	245.0	-0.05	4.54	0.90	0.324
838	3.99	248.3	-0.01	3.66	0.96	0.350
906	2.42	221.5	0.00	1.90	0.88	0.369
1100	7.46	288.0	-0.01	7.20	0.87	0.359
1123	7.29	283.6	-0.02	7.04	0.82	0.355
1109	7.15	271.1	-0.06	6.93	0.84	0.375
1160	5.70	268.9	-0.01	5.29	0.92	0.436
1230	3.54	239.7	-0.01	2.84	0.89	0.488
1230	3.63	242.2	-0.01	2.93	0.90	0.491
1225	3.70	231.9	-0.04	2.94	0.95	0.532
1421	7.38	285.1	-0.02	7.10	0.71	0.387
1470	7.45	291.0	0.00	7.05	0.74	0.407
1475	5.88	273.1	0.00	5.31	0.86	0.509
1475	5.87	266.6	-0.03	5.29	0.90	0.542
1475	5.63	241.2	-0.09	5.02	0.90	0.591
1475	5.60	221.7	-0.15	5.03	0.90	0.624
1475	5.59	199.7	-0.21	5.04	0.88	0.650
1475	5.56	184.3	-0.25	5.05	0.88	0.674
1475	5.57	162.0	-0.31	5.07	0.87	0.706
1480	5.53	140.2	-0.37	5.02	0.87	0.742
1480	5.50	121.8	-0.42	4.99	0.86	0.763
1480	5.44	102.8	-0.46	4.97	0.87	0.800
1480	5.52	81.0	-0.53	5.07	0.86	0.832
1485	5.41	59.2	-0.58	4.99	0.86	0.867
1480	5.39	40.4	-0.62	4.94	0.86	0.892
1496	4.81	246.6	-0.04	4.01	0.92	0.603
1518	4.69	260.4	0.00	3.90	0.87	0.552
1528	4.71	256.3	-0.01	3.90	0.92	0.598
1544	4.22	251.9	-0.01	3.31	0.87	0.576
1544	4.27	248.4	-0.02	3.30	0.90	0.604
1765	4.27	248.0	-0.02	3.00	0.91	0.695
1810	7.51	292.5	0.00	6.95	0.69	0.461
1822	5.76	222.1	-0.16	5.03	0.83	0.718
1817	5.73	204.3	-0.21	5.04	0.82	0.748
1827	5.72	179.6	-0.27	5.01	0.81	0.796
1827	5.70	159.3	-0.33	5.03	0.81	0.831
1827	5.63	141.2	-0.37	4.96	0.81	0.871
1832	5.64	119.8	-0.43	5.06	0.79	0.902
1827	5.56	102.0	-0.47	4.95	0.79	0.930
1832	5.58	80.7	-0.53	4.94	0.79	0.973
1832	5.59	60.8	-0.58	5.02	0.79	1.016
1832	5.58	38.7	-0.64	5.03	0.77	1.039
1832	5.56	22.9	-0.68	5.01	0.75	1.059
1870	5.88	276.0	0.00	5.05	0.83	0.621
1878	4.02	245.0	-0.02	2.55	0.85	0.694
2178	4.57	255.7	-0.01	3.15	0.78	0.719
2178	4.57	252.0	-0.02	3.14	0.79	0.737
2173	5.92	242.6	-0.10	5.00	0.75	0.736
2173	5.82	219.9	-0.16	4.93	0.77	0.808
2173	5.85	200.2	-0.22	5.01	0.75	0.838
2173	5.79	189.6	-0.25	5.05	0.74	0.855
2173	5.82	181.0	-0.27	5.01	0.74	0.879
2173	5.78	161.9	-0.33	5.01	0.74	0.922
2178	5.76	143.2	-0.38	4.97	0.73	0.958
2178	5.78	120.0	-0.44	5.01	0.72	1.003
2184	5.72	100.6	-0.49	5.05	0.70	1.038
2184	5.74	79.8	-0.54	5.06	0.70	1.083
2173	5.74	60.5	-0.59	5.05	0.69	1.117
2184	5.67	40.0	-0.64	5.01	0.69	1.170
2189	5.64	24.6	-0.68	4.98	0.66	1.179
2205	4.31	233.8	-0.06	2.79	0.77	0.767
2230	6.05	277.5	0.00	5.00	0.78	0.687

Table 2. Extrapolated CHF values at zero inlet quality

L m	G kg/m^{2}s	p_{out} MPa	$\dot{q}_{co}$ MW/m^2
0.240	1484	6.99	1.810
0.502	1473	7.03	0.787
0.502	2275	5.00	1.286
0.975	782	5.03	0.315
0.975	1111	7.06	0.355
0.975	1478	5.02	0.532
0.975	1828	5.01	0.615
0.975	2177	5.01	0.671

data assessed for larger diameters. In particular, for fixed diameter, length, exit pressure and inlet subcooling, CHF is an increasing function of mass flux. It is reported by Collier (1972) that for fixed D, L, G, and x_{in}, CHF reaches a maximum at low pressures (below 3 MPa) and decreases in the intermediate range from 3 to 10 MPa. This latter behaviour can be seen in Fig. 4. However, there are not enough data to draw any conclusion about the presence or the absence of the maximum at low pressure.

It is interesting to compare the CHF data from our experiments with estimates obtained from the correlations proposed by Katto and Ohno (1984), by CISE (Bertoletti *et al.* 1965) and by Bowring (see Collier 1981, pp. 265–267), even though our data lie beyond their original ranges of validity. The correlations differ substantially in kind. The Katto correlation is semi-empirical, valid for an arbitrary fluid and based on dimensionless groups. It was derived using an experimental data set covering mainly a diameter range from 3 to 11 mm. Only 3% of the data are for diameters between 1 and 3 mm (Katto 1980). The CISE correlation is empirical, extensively verified for water CHF with annular flow pattern in tubes with diameters between 7 and 25 mm. The Bowring correlation is empirical, based on the so called local condition hypothesis. It is valid for water only and its use is recommended for diameters between 2 and 45 mm. In Fig. 5 the ratio $\dot{q}_{c,calc}/\dot{q}_{c,exp}$ between predicted and experimental values of the critical heat flux is plotted versus $\dot{q}_{c,exp}$ for data with inlet quality close to zero. The Katto correlation predicts well the experimental data. The RMS error over 34 points is 8.5%. 76% of the points are correlated within ±10%. The CISE correlation seems to underpredict CHF data for diameters much smaller than the lower bound (7 mm) of its range of validity. The RMS error is 18.3%. On the other hand, the Bowring correlation overpredicts our data. The RMS error in this case is 46.7%, showing the largest scatter among the three correlations. It is noteworthy that the points which fall within the ±10% band correspond to $p_{out} \leq 4$ MPa.

In the correlations, we used p_{out} and $(h_{lg})_{out}$ for pressure and evaporation enthalpy, respectively. Correlations are usually based on the assumption that the tube pressure drop is negligible and a single pressure value is ascribed to the system. In this study, however, pressure losses are significant (up to 1.5 MPa), therefore we have also made calculations using p_{in} and $(h_{lg})_{in}$. The relative differences in the two cases are within a few percent. Therefore, pressure losses seem to have a secondary effect.

In view of the good agreement with the data, the ratio $\dot{q}_{c,calc}/\dot{q}_{c,exp}$ for the Katto correlation has been analysed also in terms of its dependence on x_{in}, G, p_{out}, and L. In Fig. 6, for example, the ratio between computed and experimental CHF is plotted versus x_{in}. Data belonging to the same series differ only in the value of x_{in}. It can be observed that the values of $\dot{q}_{c,calc}/\dot{q}_{c,exp}$ within each series of data are approximately constant. This implies that the x_{in} dependence of our data is interpreted correctly by the Katto correlation. A similar conclusion can be drawn for the pressure and the tube length dependence, although caution is necessary for the latter because of the small

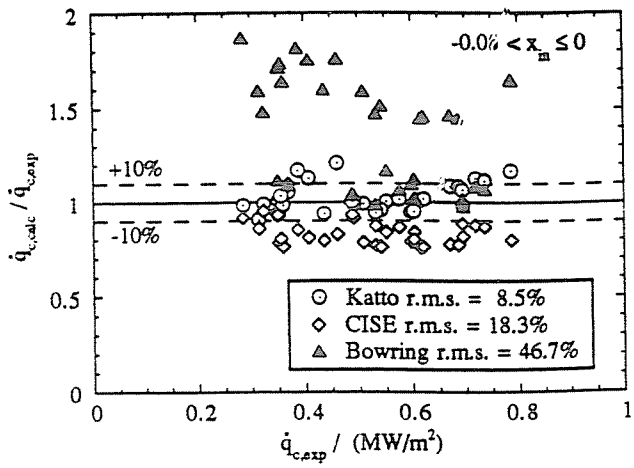

Figure 5. Comparison with extrapolations of the Katto, CISE, and Bowring correlations.

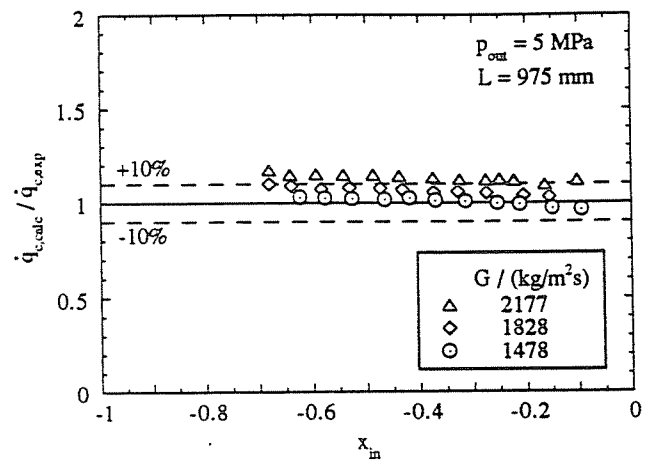

Figure 6. Comparison with extrapolations of the Katto correlation. Dependence on x_{in}.

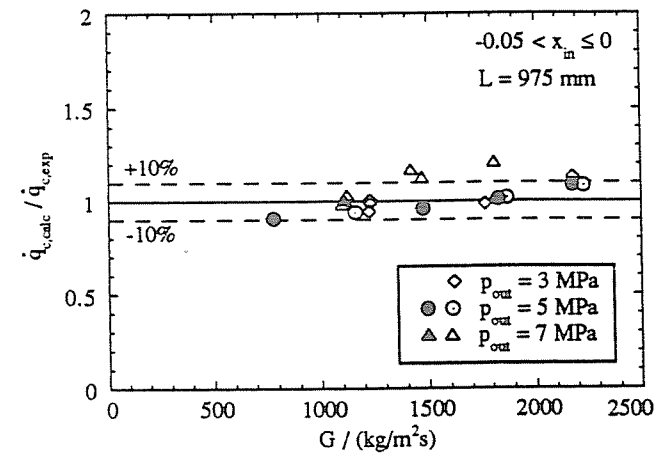

Figure 7. Comparison with extrapolations of the Katto correlation. Dependence on G. Solid marks denote extrapolated points from Table 2.

number of data available for $L = 240$ and 502 mm. About the dependence of $\dot{q}_c$ on G, our data seem to behave in a slightly different way from that predicted by the Katto correlation. As is seen in Fig. 7, the experimental values of $\dot{q}_c$ show a tendency to increase more slowly with the mass flux.

The good agreement of the measured CHF data with the values calculated using the Katto correlation for water in 1 mm i.d., long tubes, allows some interesting considerations on the CHF pattern found in the present study. The Katto correlation predicts the CHF for three characteristic regimes, i.e., the L-regime which occurs for low mass flux, the N-regime for high mass flux, and the intermediate H-regime (Katto 1980). In the L- and H-regime, the flow pattern at the tube exit is spray annular, whereas in the N-regime the flow is bubbly. Moreover, CHF is due to liquid film dryout on the heated wall in the L-regime, and to liquid film breakdown in the H-regime, whereas it is closely related to DNB in the N-regime. The boundary between the H- and the N-regime is given by the equation

$$\frac{\sigma\rho_l}{G^2 L} = \left(\frac{0.77}{L/D}\right)^{2.7}$$

For all our CHF data, the value of $\sigma\rho_l/G^2L$ is about 100 times higher than the boundary value between the H- and the N-regime, i.e., the data lie well within the L-regime. This is in agreement with the small mass flux G and high exit quality x_{out} that characterize the data presented, and confirms that the flow pattern is annular. Moreover, the L-regime is characterized by a CHF reached by liquid film dryout rather than its rupture; and this agrees with the very smooth, nondestructive and reversible CHF conditions observed in the present study.

5. CONCLUSIONS

In this work experimental data for CHF in horizontal capillary tubes are presented. The data characterized by high exit quality values, were collected at various values of pressure, mass flux, inlet subcooling, and tube length. The data show a qualitative agreement with CHF behaviour in tubes with larger diameters. There is also quantitative agreement with predictions from the Katto correlation.

We conclude that, for low mass fluxes, high L/D ratios and tube diameters down to 1 mm, the effect of tube diameter on CHF does not seem to differ from that characteristic of larger diameters. However, work is still needed to confirm this result. For example, larger mass fluxes should be investigated in order to extend the analysis for other flow regimes. Again, data for other tube diameters smaller than 1 mm should be collected.

ACKNOWLEDGEMENTS

The authors are indebted to Prof. M. Silvestri of the Politecnico di Milano who provided invaluable guidance and insights in defining the project and designing the apparatus, and to A. Rapagna and A. Tortelli who helped in performing the experimental runs. The work was supported by MURST via 60% and 40% grants to the Università di Brescia and the Politecnico di Milano.

REFERENCES

Bergles, A.E. 1963, Subcooled Burnout in Tubes of Small Diameter, ASME Paper 63-WA-182.

Bertoletti, S., Gaspari, G.P., Lombardi, C., Peterlongo, G., Silvestri, M. & Tacconi, F.A. 1965, Heat Transfer Crisis with Steam-Water Mixtures, Energia Nucleare, vol. 12, pp. 121–172.

Celata, G.P. 1993, Recent Achievements in the Thermal Hydraulics of High Heat Flux Components in Fusion Reactors, Exp. Thermal Fluid Sci., vol. 7, pp. 177–192.

Collier, J.G. 1981, Convective Boiling and Condensation, 2nd ed., pp. 248–274, McGraw-Hill, New York.

Echigo, R., Yoshida, H., Hanamura, K. & Mori, H. 1992, Fine-Tube Heat Exchanger Woven with Threads, Int. J. Heat Mass Transfer, vol. 35, pp. 711–717.

Hosaka, S., Hirata, M. & Kasagi, N. 1990, Forced Convective Subcooled Boiling Heat Transfer and CHF in Small-Diameter Tubes, Proc. 9th Int. Heat Transfer Conf.,Jerusalem, vol. 2, pp. 129–134.

Katto, Y. 1980, General Features of CHF of Forced Convection Boiling in Uniformly Heated Vertical Tubes With Zero Inlet Subcooling, Int. J. Heat Mass Transfer, vol. 23, pp. 493–504.

Katto, Y. & Ohno, H. 1984, An Improved Version of the Generalized Correlation of Critical Heat Flux for the Forced Convective Boiling in Uniformly Heated Vertical Tubes, Int. J. Heat Mass Transfer, vol. 27, pp. 1641–1648.

Mishima, K., Nishihara, H., Kureta M. & Tasaka, K. 1993, Critical Heat Flux for Low Pressure Water in Small Diameter Tubes, Proc. 6th Int. Topical Meeting on Nuclear Reactor Thermal Hydraulics, Grenoble, vol. 1, pp. 435–443.

Weisman, J., Duncan, D., Gibson, J. & Crawford, T. 1979, Effects of Fluid Properties and Pipe Diameter on Two-Phase Flow Patterns in Horizontal Lines, Int. J. Multiphase Flow, vol. 5, pp. 437–462.